A&A 549, A29 (2013)
DOI: 10.1051/0004-6361/201219696

Astronomy & Astrophysics

The VMC Survey

VI. Quasars behind the Magellanic system⋆

M.-R. L. Cioni[1,2,⋆⋆], D. Kamath[3], S. Rubele[4], J. Th. van Loon[5], P. R. Wood[3], J. P. Emerson[6], B. K. Gibson[7], M. A. T. Groenewegen[8], V. D. Ivanov[9], B. Miszalski[10,11], and V. Ripepi[12]

[1] University Observatory Munich, Scheinerstrasse 1, 81679 München, Germany
e-mail: mcioni@usm.uni-muenchen.de
[2] University of Hertfordshire, Physics Astronomy and Mathematics, Hatfield AL10 9AB, UK
[3] RSAA, Mount Stromlo Observatory, Cotter Road, Weston Creek, ACT 2611, Australia
[4] INAF, Osservatorio Astronomico di Padova, Vicolo dell'Osservatorio 5, 35122 Padova, Italy
[5] Keele University, Lennard-Jones Laboratories, ST5 5BG, UK
[6] School of Physics and Astronomy, Queen Mary University of London, Mile End Road, London E1 4NS, UK
[7] Jeremiah Horrocks Institute, University of Central Lancshire, Preston PR1 2HE, UK
[8] Royal Observatory of Belgium, Ringlaan 3, 1180 Ukkel, Belgium
[9] European Southern Observatory, Av. Alonso de Córdoba 3107, Casilla 19, Santiago, Chile
[10] South African Astronomical Observatory, PO Box 9, 7935 Observatory, South Africa
[11] Southern African Large Telescope Foundation, PO Box 9, 7935 Observatory, South Africa
[12] INAF, Osservatorio Astornomico di Capodimonte, via Moiariello 16, 80131 Napoli, Italy

Received 28 May 2012 / Accepted 10 October 2012

ABSTRACT

Context. The number and spatial distribution of confirmed quasi-stellar objects (QSOs) behind the Magellanic system is limited. This undermines their use as astrometric reference objects for different types of studies.
Aims. We have searched for criteria to identify candidate QSOs using observations from the VISTA survey of the Magellanic Clouds system (VMC) that provides photometry in the YJK_s bands and 12 epochs in the K_s band.
Methods. The $(Y - J)$ versus $(J - K_s)$ diagram has been used to distinguish QSO candidates from Milky Way stars and stars of the Magellanic Clouds. Then, the slope of variation in the K_s band has been used to identify a sample of high confidence candidates. These criteria were developed based on the properties of 117 known QSOs presently observed by the VMC survey.
Results. VMC YJK_s magnitudes and K_s light-curves of known QSOs behind the Magellanic system are presented. About 75% of them show a slope of variation in $K_s > 10^{-4}$ mag/day and the shape of the light-curve is in general irregular and without any clear periodicity. The number of QSO candidates found in tiles including the south ecliptic pole and the 30 Doradus regions is 22 and 26, respectively, with a ∼20% contamination by young stellar objects, planetary nebulae, stars and normal galaxies.
Conclusions. By extrapolating the number of QSO candidates to the entire VMC survey area we expect to find about 1200 QSOs behind the LMC, 400 behind the SMC, 200 behind the Bridge and 30 behind the Stream areas, but not all will be suitable for astrometry. Further, the K_s band light-curves can help support investigations of the mechanism responsible for the variations.

Key words. surveys – Magellanic Clouds – quasars: general – infrared: galaxies

1. Introduction

The astrometric accuracy and the photometric sensitivity of observations made with VISTA is sufficiently good that we expect data from the VISTA Magellanic Clouds survey (VMC; Cioni et al. 2011, hereafter Paper I) can be used to derive proper motions of the Magellanic Clouds (MCs). Such proper motion studies require a reference grid of bright, distant, non-moving, point like objects. Quasi-stellar objects (QSOs) provide such a grid (e.g. Kallivayalil et al. 2006; Costa et al. 2011). QSOs are point-like sources believed to be powered by accretion onto black holes in the centre of distant galaxies. QSOs can also be used as background sources to examine the composition of the MC interstellar medium along the line of sight (e.g. Redfield et al. 2006; van Loon et al. 2009), and are important for studies of galaxy formation and evolution.

The density of QSOs with $i < 19$ mag is ∼11 per deg^2 as estimated from the Sloan Digital Sky Survey (SDSS) Quasar Catalogue (Schneider et al. 2010) but discovery of candidate QSOs behind the MCs is complicated by the necessity to distinguish candidate QSOs from the dense stellar content of the MCs themselves. Candidate QSOs must then be observed spectroscopically to confirm which are true QSOs, and to make this process efficient the sample of candidate QSOs should be as clean as possible. Selection of candidate QSOs behind the MCs has been greatly improved by long-term multi-epoch observations, as part of micro-lensing projects such as the MAssive Compact Halo Objects (MACHO – Alcock et al. 2000) and the Optical Gravitational Lensing Experiment (OGLE – Udalski et al. 1992), and using data at various wavelengths, from ultraviolet (UV) to infrared (IR), that permit better

⋆ Based on observations made with VISTA at the Paranal Observatory under program ID 179.B-2003.
⋆⋆ Research Fellow of the Alexander von Humboldt Foundation.

removal of stellar objects (young stellar objects, planetary nebulae, hot and red stars) from QSO candidate samples. Methods used to identifying candidate QSOs include X-ray (Shanks et al. 1991) or radio emission (Schmidt 1968), mid-IR (Stern et al. 2005) and near-IR colours (see below). Flux variations probably associated with the accretion disc have also been used (Hook et al. 1994). QSO candidates are spectroscopically confirmed on the basis of optical and UV ionic emission lines, from which their redshifts are measured (e.g. Vanden Berk et al. 2001). The most recent such investigation by Kozłowski et al. (2012) focused on the southern edge of the Large Magellanic Cloud (LMC) and is relatively complete for objects with $I < 19.2$ mag, with a candidate sample based on *Spitzer* Space Telescope mid-IR colours, X-ray emission and/or optical variability. Spectra of their sample quadrupled the number of confirmed QSOs behind the LMC.

Currently there are 360 known QSOs behind the Magellanic system of which 233 are behind the LMC, 100 behind the Small Magellanic Cloud (SMC) and 27 behind the inter-cloud region including the Magellanic Bridge, and many more QSO candidates awaiting follow-up observations to establish their nature (e.g. Kozłowski & Kochanek 2009; Kim et al. 2012). However these objects cover a limited area compared to the extent of the whole MC system being surveyed in the VMC survey. VMC detects sources as faint as $K_s = 23.4$ mag (AB) with $S/N = 5$, corresponding to the luminosity of sources below the old main-sequence turnoff in the LMC which occurs at $I \sim 22$ mag. The YJK_s VMC survey, which is multi-epoch in K_s, has the potential to considerably enlarge the parameter space for the search of QSOs, behind the Magellanic system, both in terms of sensitivity and spatial distribution. Near-IR criteria to select QSOs have been proposed previously. Kouzuma & Yamaoka's (2010) criteria were based on 2MASS JHK bands. A series of papers have described the K excess (KX) method (Warren et al. 2000) using UKIDSS JK bands and the SDSS g band (e.g. Maddox et al. 2012; Mortlock et al. 2012). Findlay et al. (2012) based their selection on single epoch VISTA ZYJ data.

Our aim is to establish VMC YJK_s bands selection criteria using the known QSOs behind the Magellanic system which have already been observed, and investigate their utility in identifying new candidate QSOs in the areas being surveyed. The first stage of our method uses the $(Y - J)$ vs. $(J - K_s)$ diagram and the second stage uses K_s variability.

Section 2 describes the VMC data for the known QSOs behind the Magellanic system that have been covered so far. Section 3 uses VMCs YJK_s photometry of these QSOs to establish colour criteria for isolating them from Milky Way (MW) and MC objects, and to examine the K_s variability of the QSOs over a baseline of up to 12 epochs over two years. Section 4 discusses the reliability of our method and Sect. 5 presents our conclusions. The appendix provides further information on the known QSOs and their K_s band light-curves. The influence of reddening and of photometrically selected non-QSOs on our selection criteria is also discussed in there.

2. Data and sample

2.1. VMC data

The near-IR data analysed in this study were obtained with the Visual and Infrared Survey Telescope for Astronomy (VISTA; Emerson & Sutherland 2010) for the VMC survey and include observations acquired until the end of September 2011. The data were reduced onto the VISTA photometric system (Vegamag = 0) with the VISTA Data Flow System (VDFS) pipeline v1.1 (Irwin et al. 2004) and extracted from the VISTA Science Archive[1] (VSA). The survey strategy involves repeated observations of tiles, where one tile homogeneously covers an area of 1.5 deg^2 with 3 epochs in both Y and J filters, and 12 epochs in K_s with the epochs spread over a time range of a year or longer. Details about the observing strategy and the data reduction are given in Paper I.

Table 1. VMC tile sensitivity and epochs.

Tile	Limiting magnitude[a]			Epochs
	Y (mag)	J (mag)	K_s (mag)	K_s
SMC 3_3	20.659	20.412	19.607	9
SMC 3_5	21.127	21.002	19.693	10
SMC 4_3	20.152	19.977	19.071	3
SMC 5_4	20.678	20.461	19.621	11
BRI 2_3	21.222	20.952	19.734	9
BRI 3_7	20.972	20.742	18.418	1
LMC 4_2	21.305	20.593	19.501	8
LMC 4_6	20.652	20.378	18.587	2
LMC 5_5	19.890	19.626	19.081	10
LMC 6_4	19.259	18.962	18.576	10
LMC 6_6[b]	19.906	19.514	18.995	14
LMC 6_8	20.782	20.585	17.911	1
LMC 7_3	20.406	19.949	18.802	2
LMC 8_3	20.882	20.364	19.676	12
LMC 8_8[b]	21.091	20.760	19.856	14
LMC 9_7	20.989	20.414	18.226	1

Notes. [(a)] For sources with photometric error <0.1 mag. [(b)] VMC observations are completed.

Table 1 lists the tiles that contain known QSOs and for which observations were obtained by end of September 2011. Tile names are specified in Col. 1 and the limiting magnitude corresponding to sources with photometric errors <0.1 mag in Cols. 2–4 while the number of available K_s epochs is given in Col. 5 (see also Sect. 3.4).

VMC sources have numerical quality flags and in the following analysis we discriminate sources that are well detected (Flag A – with quality flags =0−16 where 16 indicates that a source has been de-blended in at least one wave band), and those with a low quality detection (Flag B – with quality flags >16 that would arise if a source is located in the under-exposed edge areas of a tile, or in the upper half of detector #16 which is known to have a varying quantum efficiency, that may result in bad flat fielding and unreliable magnitudes, or has a low confidence in the aperture magnitude).

2.2. Known quasars

The spatial distribution of the 360 spectroscopically confirmed QSOs behind the Magellanic system is shown in Fig. 1. Most of them, confirmed prior to July 2009, are included in the compilation by Véron-Cetty & Véron (2010) and we use their coordinates, corrected according to Flesch (2012), instead of those from the original studies. The lists of QSOs behind the LMC and SMC are discussed in Sects. A.1 and A.2, respectively. For the presently studied VMC dataset only 117 quasars are included within the regions observed by the VMC survey, with most of them contained in tiles LMC 5_5, LMC 6_4, SMC 4_3

[1] http://horus.roe.ac.uk//login.html

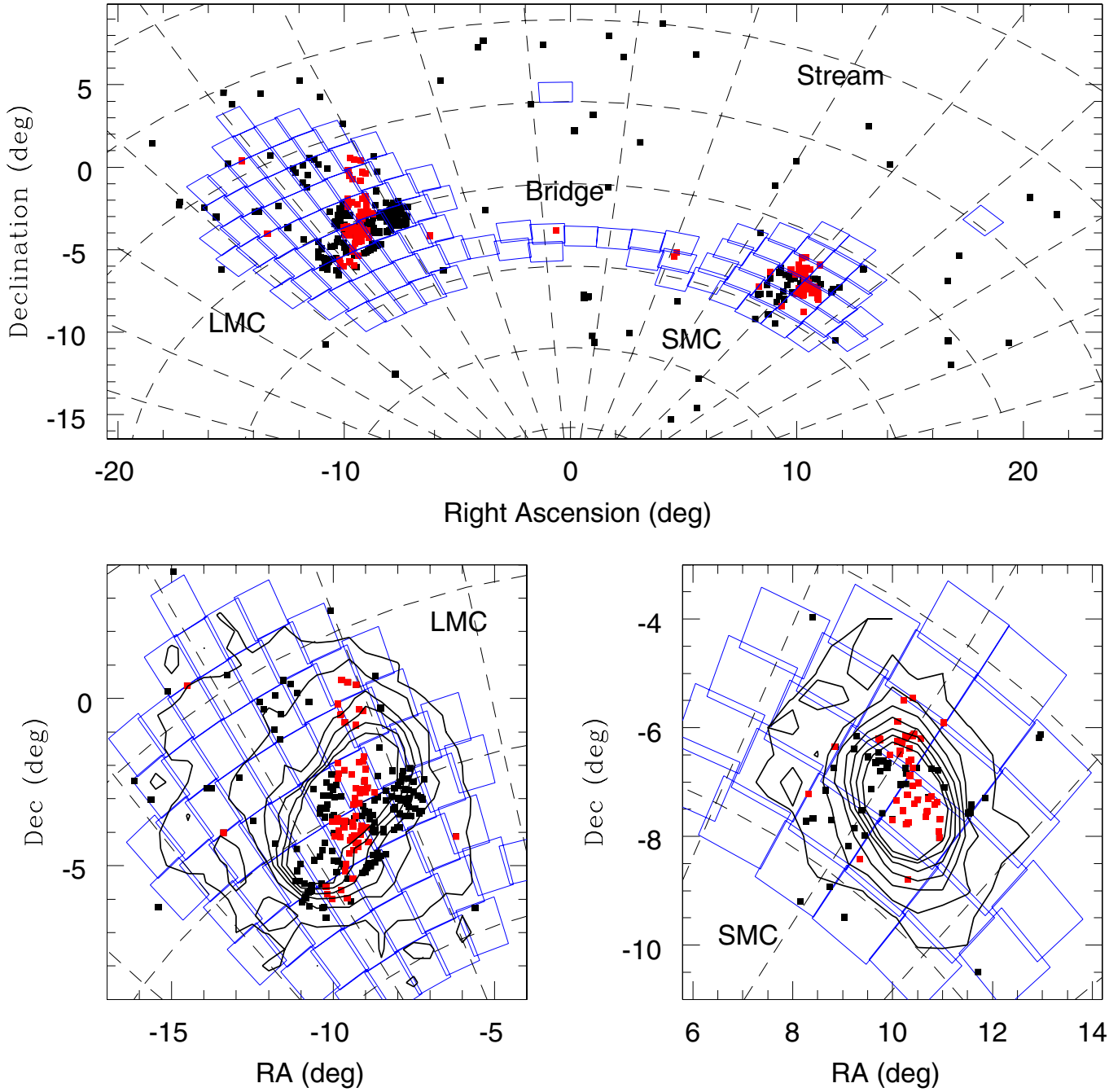

Fig. 1. Distribution of known quasars behind the Magellanic system (*top*) with enlargements on the LMC (*bottom-left*) and SMC (*bottom-right*). All known quasars are shown with filled small black squares while those positionally matched with presently available VMC data are shown in red. Large empty blue rectangles indicate the VMC tiles. Contour plots show the distribution of evolved giant stars which delineate the outer structure and bar of the galaxies. Coordinates are given with respect to $(\alpha_0, \delta_0) = (51°, -69°)$.

and SMC 5_4. Tile numbering begins from the bottom right corner, increasing from right to left and from bottom to top. The first LMC tile is 2_3, the first SMC tile is 2_2, the first Bridge tile is 1_2 and Stream tile 1_1 is right above the Bridge while 2_1 is to the right of the SMC. The central coordinates of VMC tiles are given in Paper I while the contour plots showing the outer structure and bar of the galaxies as well as the distribution of evolved giant stars are described in Cioni et al. (2000).

Figure 1 shows that the distribution of known QSOs is inhomogeneous and biased to the central region of the galaxies. This is because most QSOs were extracted from micro-lensing surveys that have focused their observations on the densest regions, i.e. the bar of the galaxies. In addition, not all candidates from these searches have been spectroscopically followed-up, further limiting the area with known QSOs.

2.3. Cross-correlation

VMC detections of the 126 known (spectroscopically confirmed) QSOs covered by VMC data up to September 2011 were selected by searching for the nearest counterpart within 2″. This produced 117 matches in the merged catalogue ("vmcsource") containing Y, J and K_s band sources extracted from "tiledeepstacks" which are deep tile images resulting from the

Table 2. VMC quasar parameters.

Name	Ref.	α (h:m:s)	δ (d:m:s)	Y (mag)	σ_Y (mag)	J (mag)	σ_J (mag)	K_s (mag)	σ_{K_s} (mag)	Class	Tile	Flag
OGLE 003850.79−731053.1	3	00:38:50.80	−73:10:53.4	16.562	0.006	16.142	0.006	14.878	0.006	−1	SMC 4_3	A
J003857.50−741000.7	10	00:38:57.53	−74:10:00.9	17.371	0.010	17.104	0.010	16.449	0.0123	−1	SMC 3_3	A
J003957.65−730603.6	7	00:39:57.64	−73:06:03.6	18.321	0.022	18.334	0.026	16.900	0.019	1	SMC 4_3	A

References. (1) Dobrzycki et al. (2002); (2) Geha et al. (2003); (3) Dobrzycki et al. (2003a); (4) Dobrzycki et al. (2003b); (5) Dobrzycki et al. (2005); (6) Véron-Cetty & Véron (2010); (7) Kozłowski et al. (2011); (8) Kozłowski et al. (2012); (9) Tinney et al. (1997); (10) Kamath et al. (in prep.).

combination of individual tile images taken at different observing epochs. A further 8 QSOs were matched in the un-merged catalogue, and only one QSO was undetected. We inspected the images of all 126 objects and most were good and well matched to counterparts at <1″, see Sect. A.3 for details.

Table 2 (electronically available) lists the VMC data for the 117 known quasars (three are shown as an example). The first column gives the QSOs name from the literature for which references are in Col. 2. Columns 3 and 4 list the J2000 coordinates of the VMC counterparts. The Y, J and K_s magnitudes and 1 sigma uncertainties are listed in Cols. 5–10. Column 11 lists the VDFS source classification flag (1 for galaxies, −3 for probable galaxies, −1 for stars and −2 for probable stars), Col. 12 the VMC tiles where QSOs were found and Col. 13 the Flag (see Sect. 2.1).

Of the 117 matched QSOs, 67 lie behind the LMC, 47 behind the SMC and 3 behind the Bridge regions. The majority of the QSOs are detected in all three wave bands, with 1 QSO present only in YJ data, 3 only in JK_s data and 2 only in K_s data. The VDFS pipeline classifies ∼53% of the matched QSOs as galaxies and the other 47% as stars or probable stars.

For the 8 QSOs detected in the un-merged VMC catalogue, but blended with other sources which appear in the VMC merged catalogue, Table 3 lists the name, reference, wave bands and VMC tile in Cols. 1–4, respectively. These objects are not used in our analysis.

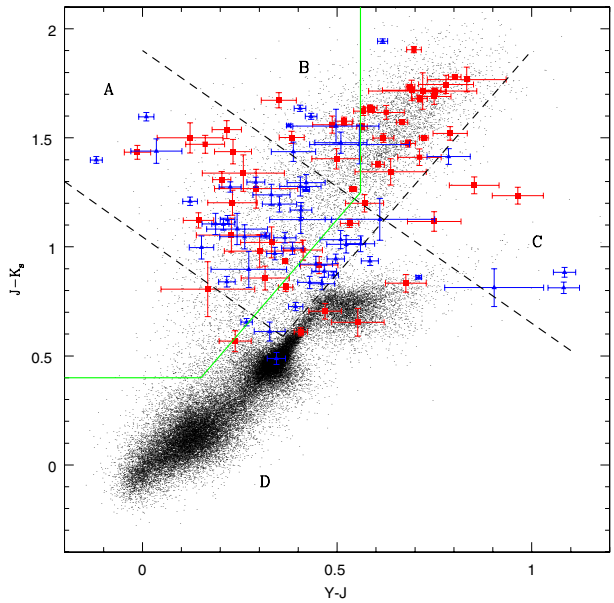

Fig. 2. Colour–colour diagram showing the known QSOs classified as galaxy-like (red filled squares) and as star-like (blue filled triangles) in the VMC data. Sources from the LMC tile 8_8 with photometric errors <0.1 mag and quality flags =0 in each wave band are shown with black dots. Dashed black lines identify the regions where known QSOs are found while the green line encloses the region with PNe.

3. Results

3.1. YJK_s colour–colour diagram and known QSOs

Figure 2 shows the distribution of the 117 known QSOs in the YJK_s colour–colour diagram superimposed to the distribution of sources detected in the LMC tile 8_8. This tile was chosen for comparison because it is located in the disc of the LMC, where crowding influences the detection of sources rendering the sample with small photometric errors shallower than in the outer regions. In addition, the VMC data for this tile are complete. All 117 known QSOs are shown regardless of their quality flag and we have checked that the analysis of this paper does not change if only QSOs with Flag A (Sect. 2.1) are used. Most QSOs are located within the triangle limited by the following lines and the plotted region:

$$(J - K_s) = -1.25 \times (Y - J) + 1.05 \quad (1)$$

$$\text{and } (J - K_s) = 2.05 \times (Y - J) - 0.15 \quad (2)$$

$$\text{where the line } (J - K_s) = -1.25 \times (Y - J) + 1.90 \quad (3)$$

marks the division between star-like (region A) and galaxy-like (region B) QSOs. This line is parallel to the first line (Eq. (1)) that defines a blue colour boundary beyond which no known QSOs are present. The other line (Eq. (2)) runs parallel to the locus of stars and divides them from extra-galactic sources. Some known QSOs have colours outside the triangular area which is divided into regions C and D by prolonging the line defined by Eq. (3). The selection criteria that embrace the sample of known QSOs are not influenced by the choice of tile for the foreground sources, which are only shown for the purpose of visualisation or by reddening (Sect. A.4).

Among other objects populating the colour–colour space, the highest concentrations of non-QSOs are attributed to main-sequence stars at the bluest colours and to giant stars of the LMC. The plume of sources with $(Y - J) > 0.5$ mag belongs to the MW. Source at $(Y - J) \sim 0.6$ mag and $(J - K_s) \sim 1.5$ mag are mostly background galaxies. Of the total number of QSOs occupying region A, 65% are classified as star-like in VMC data and 35% as galaxy-like. QSOs in region B have the opposite distribution, with 21% classified as star-like and 79% as galaxy like. Many of the star-like QSOs are redder than the green sloped line delimiting the region where most planetary nebulae (PNe) are found (Miszalski et al. 2011a, hereafter Paper II). Only a handful of QSOs occupy region C, but the number of sources in this region does increase in the presence of interstellar reddening, e.g. in tile LMC 6_6 (Table 4). The number of QSOs located in

Table 3. VMC blended quasars.

Name	Ref.	Filter	Tile
J004753.62−724350.6	7	K_s	SMC 4_3
J005444.70−724813.7	7	K_s	SMC 4_3
J005714.13−723342.8	7	K_s	SMC 5_4
MQS J051944.39−701957.3	8	J, K_s	LMC 5_5
MQS J052300.14−701831.7	8	Y, K_s	LMC 5_5
MQS J052431.88−702231.6	8	K_s	LMC 5_5
MQS J052908.79−702445.7	8	J, K_s	LMC 5_5
MQS J053304.31−714848.4	8	K_s	LMC 4_6

Notes. References as in Table 2.

region D, that cannot be distinguished from LMC and MW stars by their colours, is small. QSOs in regions C and D are half classified as star-like and half as galaxy-like.

The YJK_s colour–colour diagram (Fig. 2) represents the best VMC diagram to distinguish the bulk of background QSOs from the foreground stellar population of the MCs and the MW. It also provides a clear indication of the location of normal galaxies. We note that our colour selection is analogous to the initial criterion in the KX QSO selection method by Maddox et al. (2012) which uses gJK, but with the g band replaced by the Y band. For a similar distribution in the VJK colour–colour diagram see Warren et al. (2000).

3.2. YJK_s colour–colour diagram and QSO models

QSO templates obtained from *Spitzer*-space-telescope Wide-field InfraRed Extragalactic (SWIRE) project template library by Polletta et al. (2007) have been convolved with the VISTA spectral response over each of the YJK_s filters and the location of these QSOs is shown in Fig. 3. The template models are semi-empirical, i.e. they have been constructed combining observational data for similar objects. Those used here refer to three type 1 QSOs, one type 2 QSO and two obscured QSOs as well as a moderately luminous AGN. Regions A+B where most known QSOs are found are well matched by the models. The average redshift from the QSO models (excluding I19254 and Sey 1.8) is 1.22 ± 0.25 in region A and 0.44 ± 0.25 in region B. This is consistent with the trends presented in Sect. A.5.

3.3. Colour–magnitude diagrams

The distribution of known QSOs in the colour-magnitude diagrams (CMDs) is shown in Fig. 4 superimposed on the distribution of LMC and MW sources present in tile LMC 8_8.

The $(Y - J)$ vs. Y or J CMDs show that QSOs overlap with the stellar populations of the LMC and MW. The $(Y - K_s)$ vs. Y or K_s CMDs provide the best separation between the LMC and MW stars as well as background galaxies. QSOs, especially those with a stellar morphology, overlap with MW stars. The $(J - K_s)$ vs. J or K_s CMDs offer instead the best separation between QSOs and stars of the MW or LMC. In the $(J - K_s)$ vs. K_s CMD, galaxy-like QSOs overlap with the cone of galaxies (with base $1 < (J - K_s) < 2$ mag and vertex at $(J - K_s) \sim 1.5$ mag); see Kerber et al. (2009), while star-like QSOs seem well separated from it.

Known QSOs in the CMDs unsurprisingly indicate that the present sample is magnitude limited and that the VMC data potentially finds candidates fainter by >1 mag.

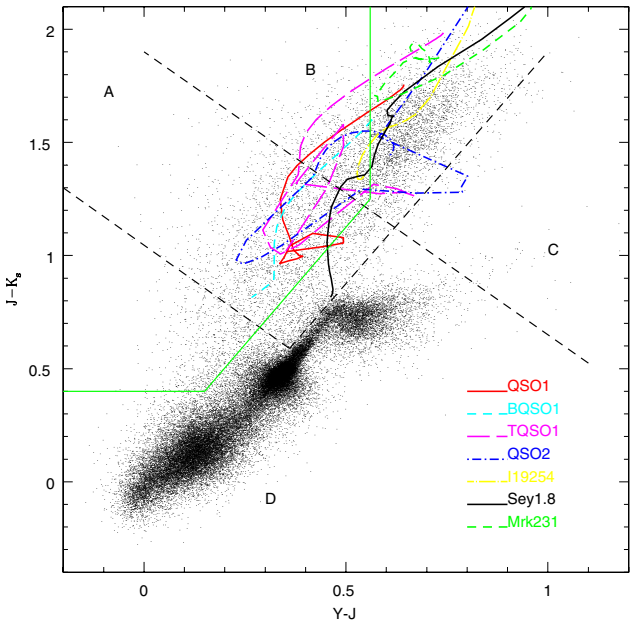

Fig. 3. Colour–colour diagram showing models from the SWIRE template library (Polletta et al. 2007) and sources as in Fig. 2.

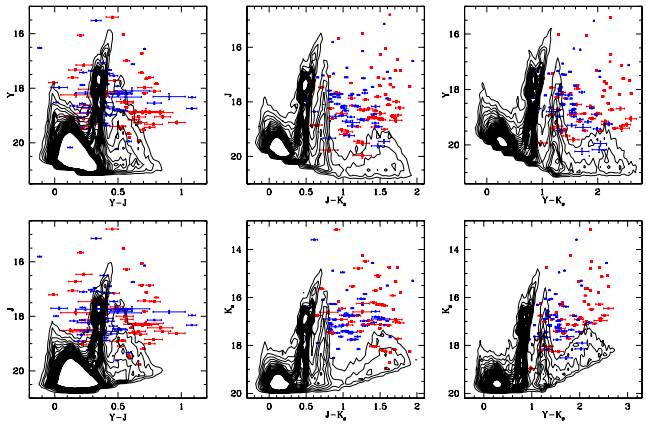

Fig. 4. Hess diagrams of sources in tile LMC 8_8 with photometric errors <0.1 mag and quality flags =0, in each pair of two wave bands, shown as contour plots. The known QSOs behind the Magellanic system are displayed as squares. QSOs are colour coded as in Fig. 2.

3.4. Variability from K_s photometry

The VMC survey provides at least 12 epochs in K_s observed under similar observing conditions (Paper I). Additional epochs may, however, be obtained in worse conditions. The number of epochs currently available (Table 1) is not sufficient to sample in detail a QSO light-curve but the accuracy of the photometry is enough to detect significant variability.

The light-curves for each known QSO from the presently available VMC data are shown in Sect. C, Fig. 5 shows one example. Good measurements obtained during the same night have been averaged and the error bar corresponds to the standard deviation of the mean. We refer to the 39%, 27% and 33% of the known QSO light-curves sampled over 300–600 days, 40–80 days and shorter days as the long, mid and short-range samples, respectively. The current short sample includes some single epoch observations.

The shapes of the light-curves are in general irregular without any clear periodicity. There is often a change in brightness as a function of time both in the long- and mid-range samples.

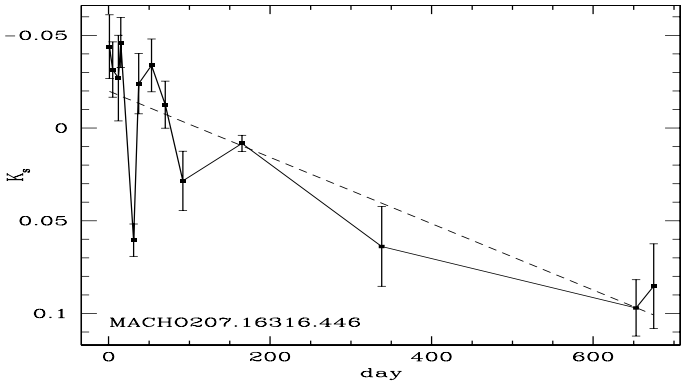

Fig. 5. Mean K_s band QSO variation. Nightly averaged points are connected by a continuous line while a dashed line represents a linear fit through them. Error bars are the standard deviations from the mean. The slope of the line is $1.8 \pm 0.4 \times 10^{-4}$ mag/day where day 0 corresponds to the first observation in the VMC data.

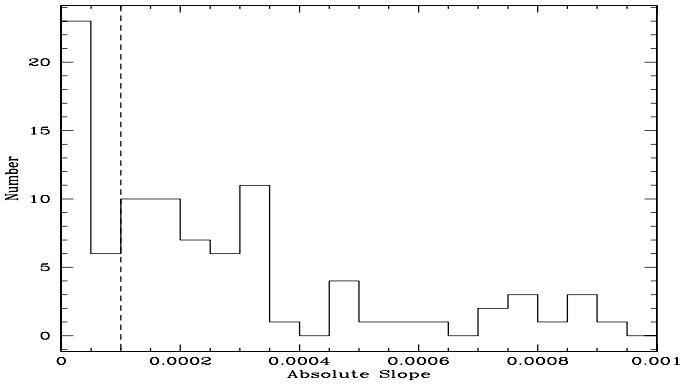

Fig. 6. Number of QSOs as a function of slope of variation in the K_s band. Each bin is 0.5×10^{-4} mag/day. A vertical dashed line is drawn at 10^{-4} mag/day; 75% of the QSOs have slope larger than this value.

Peaks superimposed on this trend are in some cases significant with respect to the error bars. On average there are broad (up to 100 days wide) and narrow (20–40 days wide) peaks. Curves of the mid-range sample appear noisier but this is largely an effect of the more frequent sampling compared to the long-range sample. The slope of the overall K_s variation has been derived for each known QSO and the number distribution of the slope values is shown in Fig. 6. There is a narrow peak due to sources with slope ∼0 mag/day while most of the sample has $1 <$ slope $< 3.5 \times 10^{-4}$ mag/day. Only with a larger sample of QSOs we will be able to establish if the latter is consistent with a decreasing gaussian function or represents a bump in the distribution. The remaining QSOs define a tail out to slope $\sim 10^{-3}$ mag/day. In summary ∼75% of the presently known QSOs have slope in the K_s band $> 10^{-4}$ mag/day.

3.5. Expected number of QSOs

In a given 1.5 deg^2 VMC tile we expect 17 QSOs with $i <$ 19 mag (Schneider et al. 2010). The approximate i band magnitude corresponding to a given K_s band magnitude has been calculated assuming that the ∼2.5 mag difference between the tip of the red giant branch (TRGB) at K_s and at I is applicable to other sources and that there is not a major difference between the i and I filters. The TRGB in the LMC occurs at $K_s = 12$ mag and at $I = 14.54$ mag (Cioni et al. 2000).

Tile LMC 5_5 is entirely within the area where the known QSO sample is complete to $I < 19.2$ mag (Kozłowski et al. 2012) and in this tile the faintest known QSO (MQS J051953.65−704622.7) has $Y = 19.32$, $J = 19.09$ and $K_s = 18.04$ mag. The numbers of known QSOs, the numbers of objects brighter than these limits and the fractions of known QSOs with respect to these numbers in regions A, B and C, respectively, of tile LMC 5_5 are listed in Table 4. Even with the small number statistics it is clear that galaxy-like QSOs dominate region B and star-like QSOs dominate region A.

By taking the ratio of all sources lying in colour selected regions A & B (Fig. 2) found down to the same magnitude as the faintest one and with the same photometric and quality flags to the number of known QSOs, it appears that ∼6% of all region A & B sources in tile LMC 5_5 are known QSOs. Those in region C, may be influenced by reddened LMC sources and so their percentage should be considered as an upper limit. Using this information it is possible to extrapolate the number of QSOs VMC may expect to find in the other tiles.

Using Table 4, we now analyse the other two LMC tiles for which VMC observations are completed. Tile LMC 6_6 includes the 30 Doradus regions where the reddening is the highest within the LMC implying the presence of many reddened LMC sources in region C. Tile LMC 6_6 contains more sources than tile LMC 8_8, on average, because of it is nearer to the centre of the galaxy, but the difficulty in detecting them clearly results in larger photometric errors and quality flags. This explains the inferior number of sources selected to have photometric errors <0.1 mag and quality flags =0 in each wave band (Table 4). Taking all objects in colour regions A & B and assuming the same percentage of known QSOs, as derived from tile LMC 5_5, we find the number of QSOs VMC might expect to detect, irrespective of their morphology, is 13 in tile LMC 6_6 and 30 in tile LMC 8_8 (Table 4).

3.6. QSO candidates

As 75% of the known QSOs show a variation in the K_s band with a slope $> 10^{-4}$ mag/day (Fig. 6) we expect 10 and 23 QSOs with this characteristic in tile LMC 6_6 and 8_8, respectively, among the magnitude, error and quality flag limited samples of candidates. These numbers have been confirmed by examining the light-curve variation of sources in these two tiles, for which all K_s epochs have been obtained by the VMC survey over a time range of 300–600 days.

To select objects with variability and colours like the known QSOs, we use the following criteria. Photometric errors < 0.1 mag and quality flags =0 in YJK_s, a K_s slope of variation $> 10^{-4}$ mag/day, $Y < 19.32$ mag, $J < 19.09$ mag and $K_s <$ 18.04 mag. We find a sample of 22 objects from tile LMC 8_8 of which 14, 7 and 1 are located in region A, B and C respectively (Table 4). This number is similar to the expected number of candidate QSOs derived earlier, i.e. 30 candidate QSOs are expected of which 75% (∼23) show a variation in the K_s band with a slope $> 10^{-4}$ mag/day. The same criteria applied to tile LMC 6_6 result in a sample of 26 objects, 15 and 11 in regions A and B respectively, while the large number of objects in region C reflects the contamination by reddened LMC stars (Table 4). This suggests that the combination of YJK_s colours and K_s variability selection is very effective in making a candidate QSO selection. The number of candidate QSOs would be larger if all sources of photometric class A are used (i.e. including those with 0 < quality flag <16).

Table 4. VMC quasar candidates.

Sources	Tile	Region A[a]			Region B[a]			Region C[a]		
		galaxy-like	star-like	all	galaxy-like	star-like	all	galaxy-like	star-like	all
Known QSOs	LMC 5_5	4	8	12	5	0	5	2	1	3
All sources[c]	LMC 5_5	137	29	166	140	3	143	14	21	35
QSO fraction (%)	LMC 5_5	2.9	27.6	7.2	3.6	0	3.5	14.3	4.8	8.6
All sources[c]	LMC 6_6	86	28	114	97	7	104	152[b]	845[b]	997[b]
Expected QSOs	LMC 6_6	2	8	10	3	0	3	22[b]	40[b]	62[b]
Candidate QSOs	LMC 6_6			15			11			49[b]
All sources[c]	LMC 8_8	129	55	184	317	1	318	3	12	15
Expected QSOs	LMC 8_8	4	15	19	11	0	11	0	1	1
Candidate QSOs	LMC 8_8			14			7			1

Notes. [(a)] Regions ABC are those in Fig. 2. [(b)] Includes reddened LMC stars. [(c)] Objects with $Y < 19.32$ mag, $J < 19.09$ mag and $K_s < 18.04$ mag, photometric errors <0.1 mag and quality flags =0 in each band.

4. Discussion

4.1. Non-QSO colours

Photometric criteria for selecting QSOs often result in the misclassification of sources that show similar colours and magnitudes. The main contaminants in candidate QSO samples are normal galaxies, YSOs, PNe and evolved stars. Brown dwarfs have $(Y - J) > 0.8$ mag while QSOs have $(Y - J) < 0.8$ mag (Warren et al. 2007). The cool T-type dwarfs have also $-1.5 < (J-K_s) < 0.5$ mag (Burningham et al. 2010) while L-type dwarfs have $(J - K_s) > 0.5$ mag (Knapp et al. 2004). Only the latter may be present in QSO regions BC (Fig. 2).

A list of spectroscopically confirmed non-QSOs was assembled from the investigations by Kozłowski et al. (2012), Woods et al. (2011) and Kamath et al. (in prep.). These objects were positionally matched to the VMC merged catalogue and counterparts were assigned to the nearest object within 1″. This sample comprises of 106 galaxies of which 7 are Seyferts, 41 YSOs, 9 PNe, 14 post-AGB stars, 11 blue stars (including Be stars) and 37 red stars (including AGB and red super giant stars). Ninety-four of the likely QSO candidates, with $I > 19$ mag and whose spectra are featureless and prevent a secure identification (Kozłowski et al. 2012), were also matched with the VMC data. The distribution of these sources in the colur-colour diagram is shown in Fig. 7.

Comparing Figs. 2 and 7, it seems that QSO candidates selected from the left side of the green line in regions A and B are unlikely to be contaminated by stars, galaxies or YSOs, but there will be a contamination by PNe. QSO candidates selected from region A but to the right of the green line will be contaminated by galaxies and YSOs. QSO candidates selected from region B but to the right of the green line will be contaminated by normal and Seyfert galaxies, YSOs and red stars. The sub-set of variable objects (with slope in the K_s band $>10^{-4}$ mag/day) weeds out contaminating red stars from regions B and C, and PNe from regions A and B while the distribution of galaxies and YSOs is unchanged. The distribution of objects with photometric errors <0.1 mag and quality flags =0 results in a negligible number of galaxies and YSOs in regions B and C while none remain in region A. The Kozłowski et al.'s candidate QSOs populate the colour–colour diagram similarly to known QSOs (Fig. 2) and those that remain after applying variability, photometric uncertainty and quality flag criteria, are high confidence candidates also according to our study. QSO candidates selected from region A are not influenced by QSO contaminants, but in region B five objects would not likely be QSOs. These correspond to ∼20% of the number of QSO candidates.

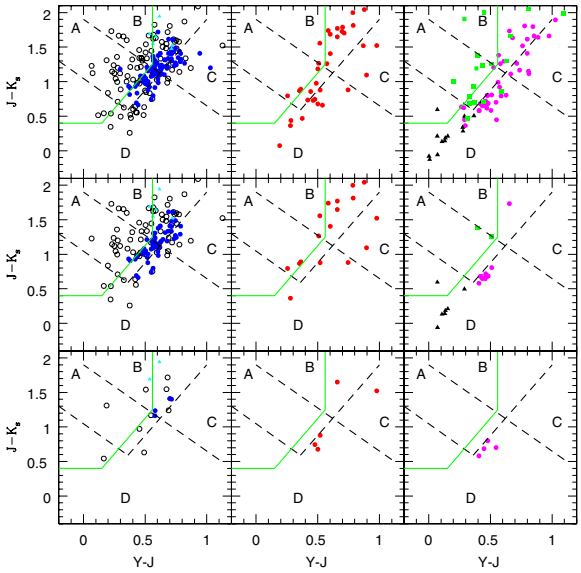

Fig. 7. Distribution of the spectroscopically confirmed non-QSOs in the colour–colour diagram from present VMC data as in Fig. B.1. (*Left column*) Likely QSOs (black circles), normal (blue circles) and Seyfert galaxies (cyan triangles). (*Middle column*) YSOs (red circles). (*Right column*) PNe and post-AGB stars (green squares), red stars (magenta circles) and blue stars (black triangles).

The influence of non-QSOs as estimated from the analysis of the photometrically selected, statistically significant whilst not entirely reliable, sample by Gruendl & Chu (2009) is described in Appendix B. Results show a 0% and 50% contamination by non-QSOs in region A and B, respectively.

A large sample of low and high confidence QSOs was obtained by Kim et al. (2012) as a result of mining the MACHO database. Initially, using a method purely based on the QSO time variability (Kim et al. 2011) and later with the additional information from observations at other wavelengths and the development of a model based on the diagnostics of known QSOs (Kim et al. 2012). Figure 8 shows the distribution of the Kim et al.'s candidate samples positionally matched with the VMC data in the colour–colour diagram. There are 574 low confidence and 179 high confidence QSOs with a VMC counterpart within 1.5″. The major point to notice is that low confidence QSOs are distributed mainly in region D while high confidence QSOs occupy mostly regions A and B. This is the case in general, for sources with a slope of variation in the K_s band $>10^{-4}$ mag/day and for sources with photometric errors <0.1 mag and quality flags =0 in

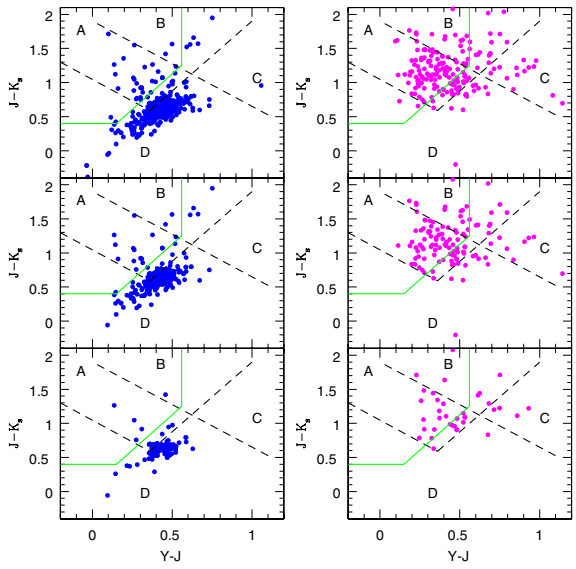

Fig. 8. Distribution of low (blue circles) and high (magenta circles) confidence QSOs in the colour–colour diagram from present VMC data as in Fig. 2.

each wave band strongly supporting the QSO selection criteria developed in this study.

4.2. QSO variability

While the optical variability of QSOs is well established (e.g. MacLeod et al. 2011) much less is known in the near-IR. The most recent investigation by Kouzuma & Yamaoka (2012) addresses the properties of the ensemble variability of QSOs using two data points from the Two Micron All Sky Survey (2MASS; Skrutskie et al. 2006) and the DEep Near-Infrared Southern sky survey (DENIS; Epchtein et al. 1999) or the UKIRT Infrared Deep Sky Survey (UKIDSS; Lawrence et al. 2007). About 15–25% of the QSO emission in the K_s band is attributed to the accretion disc (Tomita et al. 2006) and the remaining to thermal radiation by dust in the AGN torus, heated by the disc (Barvainis 1987). The reason of variations in the K_s emission may be due to changes in the inner radius of the torus as a consequence of variations in the UV/optical flux from the AGN (Koshida et al. 2009; Kawaguchi & Mori 2011).

The best sampled near-IR QSO light-curves were obtained by the Multicolour Active Galactic Nuclei Monitoring (MAGNUM) programme on NGC 4151 and NGC 5548 (Yoshii et al. 2004; Koshida et al. 2009) or focused on 3C 273 (Courvousier et al. 1988). In the first study the K light-curves of the AGN nuclei, after subtracting the contribution from the host galaxy, show clear minima and maxima each over a time range of ~200 days. Overall the K variation is smoother than the variation in the V band which appears irregular and associated with rapid variations on time scales of several days. The luminous 3C 273 source shows fast and structured flaring events also in the near-IR and only ~15 days apart. Near-IR variations of QSO emission over a time range of up to twenty years but with a sparse sampling were also found by Neugebauer et al. (1989).

The VMC multi-epoch observations represent a considerable step forward in the study of QSO near-IR variations. The present sample shows both smooth trends, i.e. an increasing and decreasing brightness over a time range of 300–600 days, and structured events, i.e. broad (up to 100 days wide) and narrow (20–40 days wide) peaks, in agreement with previous studies. In the future we plan to construct empirical template light-curves and structure functions (e.g. Hughes et al. 1992). These can then be used to refine the search for QSOs and eventually to derive their redshift as in Dai et al. (2012). A theoretical interpretation of the VMC near-IR light-curves and structure functions may also provide further evidence for the mechanism responsible for the variations and contribute to studies of the structure and dynamics of the AGN (e.g. Wold et al. 2007; Ovcharov et al. 2008).

4.3. QSO statistics

Assuming that QSOs are homogeneously distributed across the surface of the Magellanic system we can use the number of VMC candidate QSOs derived in the previous sections to estimate the total number of QSOs detectable by the VMC survey. Using the magnitude limited sample in tile LMC 8_8, which is not affected by interstellar reddening and crowding, we derived that 22 objects are candidate QSOs of which ~4 may not be true QSOs. The VMC survey comprises of 110 tiles of which 68 in the LMC, 27 in the SMC, 13 in the Bridge and 2 in the Stream areas. The expected QSO population accessible to the VMC survey is thus of at least 1200 objects behind the LMC, 400 behind the SMC, 200 behind the Bridge and 30 behind the Stream areas. This means that ~80% of the VMC accessible QSO population behind the Magellanic system is yet to be found. In addition, these numbers are conservative limits since they have originated from the application of magnitude, error, quality flag and variability restrictions. The fraction of QSO candidates suitable for astrometry, individually or as a group, will be explore in a subsequent paper.

5. Conclusions

A large sample of QSOs across the Magellanic system is of fundamental importance as an astrometric reference source for investigations of the proper motion, of the interstellar and intergalactic medium along the line of sight and to address the nature of the extra-galactic sources themselves.

We present criteria for selecting candidate QSOs based solely on the multi-epoch near-IR photometry from the VMC survey developed from the properties of 117 known QSOs. Most of them occupy two neighbouring regions of the $(Y - J)$ vs. $(J - K_s)$ diagram, one is dominated by QSOs with a star-like appearance and the other by QSOs with a galaxy-like appearance in the VMC data. The analysis of K_s multi-epochs shows that ~75% of the QSOs have a slope of variation $>10^{-4}$ mag/day across a time range up to 600 days. The combination of YJK_s colours and K_s variability criteria, with appropriate data quality flags, has been used to define samples of candidate QSOs with a ~20% contamination by non-QSOs on average, but the contamination is null in the region dominated by objects with a star-like appearance.

In LMC tile 6_6, including the 30 Doradus region, and 8_8, including the south ecliptic pole region, we find 22 and 26 QSO candidates with photometric errors <0.1 mag and quality flags =0 in each VMC wave band, brighter than 19.32, 19.09 and 18.04 mag in the Y, J and K_s band, respectively, and with a K_s slope of variation $>10^{-4}$ mag/day. The selection of QSOs from the VMC data is in excellent agreement with the sample of high confidence QSOs by Kim et al. (2012).

PNe represent the major source of contamination in the regions of the colour–colour diagram dominated by star-like QSOs

while normal galaxies and YSOs are the major contaminants in the region dominated by galaxy-like QSOs. The sub-set of sources with a slope of variation in the K_s band $>10^{-4}$ mag/day is not influenced by PNe and red stars. The sub-set of sources with photometric errors <0.1 mag and quality flags =0 in each VMC wave band is very small. Since known QSOs may be de-blended and have quality flags =16 the latter represents a reliable whilst not complete sample of candidates.

VMC magnitudes and K_s light-curves for known QSOs are provided in a table and in the appendix. The full sample of known QSOs comprises 332 QSOs from the literature and 28 newly confirmed QSOs by Kamath et al. (in prep.). VMC data on a fully observed tile in the outer LMC disc (8_8) have been used to estimate the number of QSO candidates behind the entire system as covered by the VMC survey. This is of the order of 1200 behind the LMC, 400 behind the SMC, 200 behind the Bridge and 30 behind the Stream areas. The VMC survey is the most sensitive near-IR survey of the Magellanic system to date providing for the first time near-IR counterparts to many QSOs. Spectroscopic observations of the candidates identified here will support an extension of the selection to faint magnitudes exploiting the whole VMC range available.

Acknowledgements. M.R.C. acknowledges support from the Alexander von Humboldt Foundation. This research has made use of the SIMBAD database operated at CDS, Strasbourg, France. We are grateful to ESO staff for scheduling and making the VMC observations, the Cambridge Astronomy Survey Unit and the Wide Field Astronomy Unit for providing us with the reduced data and catalogues. We thank M. I. Moretti for giving comments that improved the clarity of the paper.

References

Alcock, C., Allsman, R. A., Alves, D. R., et al. 2000, ApJ, 542, 281
Anguita, C., Patricio, L., & Pedreros, M. H. 2000, AJ, 120, 845
Barvainins, R. 1987, ApJ, 320, 537
Blanco, V. M., & Heathcote, S. 1986, PASP, 98, 635
Burningham, B., Pinfield, D. J., Lucas, P. W., et al. 2010, MNRAS, 406, 1885
Cardelli, J. A., Clayton, G. C., & Mathis, J. S. 1989, ApJ, 345, 245
Cioni, M.-R. L., Habing, H. J., & Israel, F. P. 2000, A&A, 358, L9
Cioni. M.-R. L., van der Marel, R. P., Loup, C., & Habing, H. J. 2000, A&A, 359, 601
Cioni, M.-R. L., Clementini, G., Girardi, L., et al. 2011, A&A, 527, A116 (Paper I)
Costa, E., Méndez, R. A., Pedreros, M. H., et al. 2011, AJ, 141, 136
Courvoisier, T. J.-L., Robson, E. I., Blecha, A., et al. 1998, Nature, 335, 330
Dai, D.-C., Starkman, G. D., Stojkovic, B., Stojkovic, D., & Weltman, A. 2012, Phys. Rev. Lett., 108, 231302
Dobrzycki, A., Groot, P. J., Macri, L. M., & Stanek, K. Z. 2002, AJ, 569, L15
Dobrzycki, A., Macri, L. M., Stanek, K. Z., & Groot, P. J. 2003a, AJ, 125, 1330
Dobrzycki, A., Stankek, K. Z., Macri, L. M., & Groot, P. J. 2003b, AJ, 126, 734
Dobrzycki, A., Eyer, L., Stanek, K. Z., & Macri, L. M. 2005, A&A, 442, 495
Emerson, J., & Sutherland, W. 2010, The Messenger, 139, 2
Epchtein, N., Deul, E., Derriere, S., et al. 1999, A&A, 349, 236
Eyer, L. 2002, Acta Astron., 52, 241
Findlay, J. R., Sutherland, W. J., Venemans, B., et al. 2012, MNRAS, 419, 3354
Flesch, E. 2012, PASA, accepted
Geha, M., Alcock, C., Allsman, R. A., et al. 2003, AJ, 125, 1
Girardi, L., Groenewegen, M. A. T., Hatziminaglou, E., & da Costa, L. 2005, A&A, 436, 895
Gruendl, R. A., & Chu, Y.-H. 2009, ApJS, 184, 172
Healey, S. E., Romani, R. W., Cotter, G., et al. 2008, ApJS, 175, 97
Haschke, R., Grebel, E., & Duffau, S. 2011, AJ, 141, 158
Hony, S., Kemper, F., Woods, P. M., et al. 2011, A&A, 531, A137
Hook, I. M., McMahon, R. G., Boyle, B. J., & Irwin, M. J. 1994, MNRAS, 268, 305
Hughes, P. A., Aller, H. D., & Aller, M. F. 1992, ApJ, 396, 469
Irwin, M. J., Lewis, J., Hodgkin, S., et al. 2004, SPIE, 5493, 411
Kallivayalil, N., van der Marel, R. P., Alcock, C., et al. 2006, ApJ, 638, 772
Kawaguchi, T., & Mori, M. 2011, ApJ, 737, 105
Kerber, L. O., Girardi, L., Rubele, S., & Cioni, M.-R.L. 2009, A&A, 499, 697
Kim, D.-W., Protopapas, P., Byun, Y.-I., et al. 2011, ApJ, 735, 68
Kim, D.-W., Protopapas, P., Trichas, M., et al. 2012, ApJ, 747, 107
Knapp, G. R., Legget, S. K., Fan, X., et al. 2004, AJ, 127, 3553
Koshida, S., Yoshii, Y., Kobayashi, Y., et al. 2009, ApJ, 700, L109
Kouzuma, S., & Yamaoka, H. 2010, A&A, 509, A64
Kouzuma, S., & Yamaoka, H. 2012, ApJ, 747, 14
Kozłowski, S., & Kochanek, C. S. 2009, ApJ, 701, 508
Kozłowski, S., Kochanek, C. S., & Udalski, A. 2011, ApJ, 194, 22
Kozłowski, S., Kochanek, C. S., Jacyszyn, A. M., et al. 2012, ApJ, 746, 27
Lawrence, A., Warren, S. J., Almaini, O., et al. 2007, MNRAS, 379, 1599
MacLeod, C. L., Brooks, K., Ivezić, Ž, et al. 2011, ApJ, 728, A26
Maddox, N., & Hewett, P. C. 2006, MNRAS, 367, 717
Maddox, N., Hewett, P. C., Warren, S. J., & Croom, S. M. 2008, MNRAS, 386, 1605
Maddox, N., Hewett, P. C., Péroux, C., Nestor, D. B., & Wisotzki, L. 2012, MNRAS, accepted
Meixner, M., Gordon, K., Indebetouw, R., et al. 2006, AJ, 132, 2268
Miszalski, B., Napiwotzki, R., Cioni, M.-R.L., & Nie, J. 2011a, A&A, 529, A77
Miszalski, B., Napiwotzki, R., Cioni, M.-R. L., et al. 2011b, A&A, 531, A157 (Paper II)
Mortlock, D., Patel, M., Warren, S. J., et al. 2012, MNRAS, 419, 390
Neugebauer, G., Soifer, B. T., Matthews, K., & Elias, J. H. 1989, AJ, 97, 957
Ovcharov, E. P., Nedialkov, P. L., Valcheva, A. T., et al. 2008, MNRAS, 386, 819
Perlman, E. S., Padovani, P., Giommi, P., et al. 1998, AJ, 115, 1253
Pedreros, M. H., Anguita, C., & Maza, J. 2002, AJ, 123, 1971
Polletta, M., Tajer, M., Maraschi, L., et al. 2007, ApJ, 663, 81
Redfield, S., Gibson, B. K., Thom, C., et al. 2006, AAO Newsletter, 110, 9
Schlegel, D. J., Finkbeiner, D. P., & Davis, M. 1998, ApJ, 500, 525
Schmidt, M. 1968, AJ, 151, 393
Schneider, D. P., Richards, G. T., Hall, P. B., et al. 2010, AJ, 139, 2360
Shanks, T., Georgantopoulos, I., Stewart, G. C., et al. 1991, Nature, 353, 315
Skrutskie, M. F., Cutri, R. M., Stiening, R., et al. 2006, AJ, 131, 1163
Stern, D., Eisenhardt, P., Gorjian, V., et al. 2005, ApJ, 631, 163
Tinney, C. G. 1999, MNRAS, 303, 565
Tinney, C. G., Da Costa, G. S., & Zinnecker, H. 1997, MNRAS, 285, 111
Tomita, H., Yoshii, Y., Kobayashi, Y., et al. 2006, ApJ, 652, L13
Udalski, A., Szymański, M., Kałużny, J., et al. 1992, Acta Astron., 49, 201
Vanden Berk. D. E., Richards, G. T., Bauer, A., et al. 2001, AJ, 122, 549
van Loon, J. Th., Smith, K. T., McDonald, I., et al. 2009, MNRAS, 399, 195
Véron-Cetty, M.-P., & Véron, P. 2010, A&A, 518, A10
Warren, S. J., Hewett, P. C., & Foltz, C. B. 2000, MNRAS, 312, 827
Warren, S. J., Mortlock, D. J., Legget, S. K., et al. 2007, MNRAS, 381, 1400
Wold, M., Brotherton, M. S., & Shang, Z. 2007, MNRAS, 375, 989
Woods, P. M., Oliveira, J. M., Kemper, F., et al. 2011, MNRAS, 411, 1597
Yoshii, Y., Kobayashi, Y., & Minezaki, T. 2004, Astron. Nachr., 6, 540
Zaritsky, D., Harris, J., Thompson, I. B., & Grebel, E. K. 2004, AJ, 128, 1606

Appendix A: Known QSOs behind the Magellanic system

A.1. LMC

The list of 233 spectroscopically confirmed quasars behind the LMC comprises 75 QSOs from the Véron-Cetty & Véron (2010) compilation among which 10 were identified as X-ray sources with the *Chandra* X-ray Observatory satellite and 3 as a result of mining OGLE-II light-curves (Dobrzycki et al. 2002, 2005) while 38 refer to variability in the MACHO database (Geha et al. 2003). In addition, two QSOs used by Anguita et al. (2000) and one by Pedreros et al. (2002) to study the proper motion of the LMC are attributed to a private communication by Maza in 1989 and/or do not appear in previous studies. More recently, 1 QSO was confirmed by Hony et al. (2011) and 145 QSOs by Kozłowski et al. (2012), the latter identified from OGLE-III light-curves. The entire MACHO database, with light-curves spanning a time range of ~7.5 yr, was searched by Kim et al. (2011, 2012) who trained a support vector machine model with diagnostic features based on mid-IR colours, spectral energy distribution red-shifts and X-ray luminosity of previously known QSOs to identify 663 high confidence candidates, but none of them are at present spectroscopically confirmed. Finally, as part of a spectroscopic study on post asymptotic giant branch (AGB)

stars, Kamath et al. (in prep.) confirmed 6 QSOs and detected one broad emission line in 3 additional objects that may also be QSOs.

A.2. SMC

The list of 100 spectroscopically confirmed quasars behind the SMC comprises 41 QSOs from the Véron-Cetty & Véron (2010) compilation among which 16 were discovered as counterparts to X-ray sources (Tinney et al. 1997; Tinney 1999; Dobrzycki et al. 2003b), 3 were identified from their OGLE-II light-curves (Eyer 2002; Dobrzycki et al. 2003a) and 9 from their MACHO light-curves (Geha et al. 2003). More recently, Kozłowski et al. (2011) inspected mid-IR colours from the *Spitzer* Space Telescope and the OGLE-II light-curves of sources in the central 1.5 deg^2 of the SMC. They confirmed 29 QSOs and showed broad emission lines, typical of QSOs, in 12 additional objects but the signal-to-noise ratio (S/N) in their spectra was of lower quality. The newest QSOs are from Kamath et al. (in prep.) where 17 are confirmed and 1 is a likely candidate since only one typical QSO broad emission line was detected in its spectrum.

A.3. VMC-QSO counterparts

Forty QSOs in the LMC from the list by Kozłowski et al. (2012) have counterparts at a mean separation on the sky of $0.33 \pm 0.17''$. Five matches were rejected because the corresponding VMC source, contrary to the distribution of most counterparts, was found at $>1''$ and in all five cases inspection of the VMC images showed another, fainter, object with the typical red colour of QSOs present but not found in the list of nearby objects. A cross-correlation with the "vmcdetection" un-merged catalogue shows that the likely counterparts are indeed located at $\leq 1''$ (Table 3). The counterparts to Kamath et al.'s sources have a similar separation on the sky, i.e. $0.31 \pm 0.17''$.

Seventeen QSOs were matched with the sample by Dobrzycki et al. (2002, 2003a,b, 2005) of which 7 in the SMC and 10 in the LMC. Thirty SMC QSOs were matched from the lists of Kozłowski et al. (2011); 20 from their confirmed list and 10 from their plausible list. Three matches were rejected because their detection in Y and J is suspicious; they are faint and close to a brighter object, and their suggested counterparts are at $>1.3''$ on average. The likely counterparts to these QSOs were found in the un-merged catalogue (Table 3). The VMC counterpart to QSOs J004818.76-732059.6, J004831.50-732339.9, J010057.77-722230.8 and J010137.52-720418.9 at $\sim 1''$ are perhaps affected by the extended nature of the sources since all other counterparts have a smaller separations on the sky. Four QSOs were matched with the compilation by Véron-Cetty & Véron (2010) of which 3 in the Bridge and 1 in the LMC; the latter, RXS J05466 − 6415, is the brightest near-IR quasar in the sample with $K_s = 13.590 \pm 0.004$ mag. These QSOs were originally confirmed by Perlman et al. (1998) and Healey et al. (2008) for the Bridge and LMC, respectively.

The mean separation on the sky of VMC counterparts for quasars from Dobrzycki et al. (2002, 2003a,b, 2005), Kozłowski et al. (2011) and Véron-Cetty & Véron (2010) are very similar and correspond to $0.64 \pm 0.30''$. The larger separation of VMC counterparts to the quasars from Kozłowski et al. (2011) compared to the quasars from Kozłowski et al. (2012) is most likely due to their identification from the OGLE database part II in one case and part III in the other. OGLE-II data were obtained with a CCD camera with a scale of $0.4''$/pixel while OGLE-III data were obtained with a new camera with a scale of $0.26''$/pixel and this may introduce a systematic offset in the world-coordinates between the two systems. Both OGLE surveys are well-matched to the VISTA camera which has a scale of $0.34''$/pixel.

Finally, from the list of Geha et al. (2003) 16 QSOs, of which 2 in the SMC, were successfully matched. MACHO 061.08072.0358 was excluded because two VMC candidate sources are present, one at $1.36''$ and one at $1.49''$. The mean separation on the sky of the VMC counterparts is $0.86 \pm 0.29''$.

A.4. Correction for reddening

The QSOs and stars in the MCs as well as stars in the MW are reddened by interstellar dust present along the line of sight. Reddening values in terms of $E(V - I)$ were extracted from the extinction map from Haschke et al. (2011) for all but 10 (located outside the map) of the 117 QSOs. Using the Cardelli et al. (1989) extinction law, the average QSO extinction is $A(Y) = 0.045$ mag, $A(J) = 0.032$ and $A(K_s) = 0.013$ mag. The estimated reddening, while accounting for the MW and LMC components, does not account for the intergalactic dust that lies between the LMC and the QSOs and for dust in the torus surrounding the AGN.

In tile LMC 8_8, which is outside the region studied by Haschke et al. (2011), reddening values were extracted from the Zaritsky et al. (2004) extinction map. Here, instead of dereddening each individual star, an average value referring to cool stars only, $A(V) = 0.35$ mag, was obtained in a region centred on the tile and with a radius of $12'$. Cool stars were chosen because they have similar characteristics to red clump giant and RR Lyrae stars used by Haschke et al. (2011). The size of the region, whilst being smaller than the extent of a tile, is representative of the average extinction since this tile is located in the outer disc of the LMC where the reddening is uniform. By applying the extinction law from Cardelli et al. (1989) extinction values of $A(Y) = 0.14$ mag, $A(J) = 0.10$ mag and $A(K_s) = 0.04$ mag were derived. These values may be too high since in the less populated regions of the LMC differences in $E(V-I)$ between Haschke et al. (2011) and Zaritsky et al. (2004) amount to 0.07–0.10 mag on average. In addition, while these values are applicable to LMC stars they are certainly too high towards foreground MW stars and too low towards extra-galactic sources.

In view of the uncertainty in the extinction of LMC tile 8_8, the Schlegel et al. (1998) map based on DIRBE/IRAS mid-IR observations was used to find average reddening and extinction, $E(B - V) = 0.067$ and $A(V) = 0.207$ mag, in a region of 2 deg^2 in size centred on the tile. The extinction value is consistent with the mean value, $A(V) = 0.187 \pm 0.040$ mag, derived in Paper IV from the recovering of the star formation history. $A(Y) = 0.083$ mag, $A(J) = 0.058$ mag and $A(K_s) = 0.024$ mag are then obtained. These values are 0.02–0.06 mag smaller than those derived from the Zaritsky et al. (2004) map. Using the TRILEGAL code (Girardi et al. 2005) to simulate the MW population we obtain that it accounts for $A(V) = 0.05$ of absorption implying that most of the reddening towards the LMC is due to the galaxy itself.

A.5. Trends with redshift

Figure A.1 shows the distribution of redshifts with respect to VMC magnitudes and colours. There appears to be no trend as a function of magnitude nor of $(Y - J)$ colour. The QSOs occupy

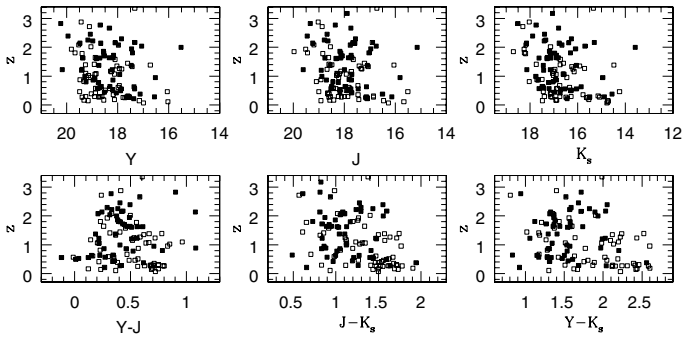

Fig. A.1. Distribution of redshift versus magnitudes (*top* line) and colours (*bottom* line) for known QSOs behind the Magellanic system. Filled symbols indicate sources classified as star-like in the VMC data and empty symbols those classified as galaxy-like.

the whole of the parameter space delimited on one side by the bright limit of the survey and on the other by the faint limit of the present sample. The faint limit is also influenced by the incomplete observations of K_s epochs.

The plots of redshift as a function of $(J - K_s)$ and $(Y - K_s)$ colours suggest a trend of larger redshifts at smaller colours. This indicates that QSOs at small redshifts are redder than QSOs at larger redshifts as predicted by Maddox & Hewett (2006). These authors found QSOs getting bluer as redshift goes from 0 to 3 in their simulations. Figure A.1 also shows a dichotomy between star-like and galaxy-like QSOs, concentrated at small redshifts as in Maddox et al. (2008).

Appendix B: Photometrically selected non-QSOs

A statistically significant sample of QSO contaminants was assembled by Gruendl & Chu (2009) who analysed spectral energy distributions, from optical to mid-IR wavelengths, and mid-IR images from *Spitzer* in the central 7° × 7° area of the LMC. Their sample has been positionally matched with the present VMC data except for their lists of probable and possible YSOs since it is indicated that the first group may be background galaxies and the second group cannot be definitely classified. The distribution of the matched sources in the colour–colour diagram is shown in Fig. B.1. There are: 286 definite and 48 probable galaxies, 396 YSOs, 25 PNe, 123 diffuse sources, 44 evolved stars and 165 stars. The majority of these sources have counterparts within ∼1″ compared to an angular resolution of *Spitzer* of ∼2″ (Meixner et al. 2006). As expected, galaxies populate region A and B but most of them are located around the line separating them from stars. This is also the preferred location of YSOs which extend to bluer colours and into region B. Most PNe are well confined in the region defined in Paper II while stars and diffuse sources occupy mostly regions C and D. A possible AGB star in the PNe region was found to be a PN by Miszalski et al. (2011a) and its colours are $(Y - J) = 0.36$ and $(J - K_s) = 2.16$ mag.

The sample of background galaxies by Gruendl & Chu (2009) contains a mixture of marginally resolved extended sources and extended sources with a point source nuclear region which were obtained from selection criteria tuned to find YSOs. They are therefore not representative of the background galaxy population in general. Among the sample of definite galaxies within the PN region Kamath et al. (in prep.) finds one QSO and one YSO out of three sources in common; the third one could not be classified due to low S/N spectral features. These

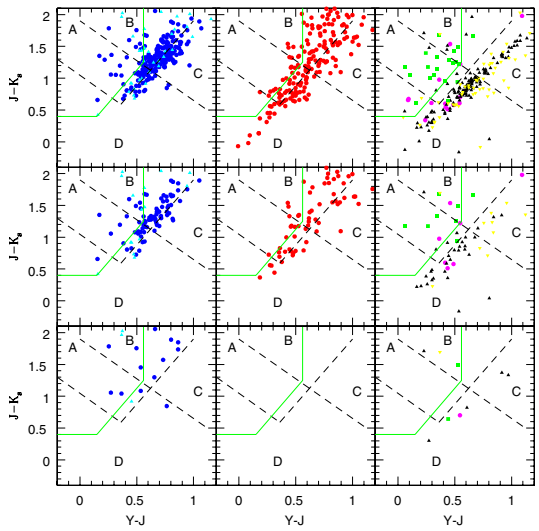

Fig. B.1. Distribution of the photometrically selected non-QSOs in the colour–colour diagram from present VMC data. (*Top* row) All positionally matched sources. (*Middle* row) Sources with a slope of variation in the K_s band $>10^{-4}$ mag/day. (*Bottom* row) Sources with photometric errors <0.1 mag and quality flags =0 in the Y, J and K_s bands. (*Left column*) Definite (blue circles) and probable (cyan triangles) background galaxies. (*Middle column*) YSOs (red circles). (*Right column*) PNe (green squares), diffuse sources (yellow reversed triangles), evolved stars (magenta circles) and other stars (black triangles). Lines are as in Fig. 2.

findings suggest that the Gruendl & Chu's classification, which is based on photometric criteria, may not be entirely reliable. Sources with a slope of variation in the K_s band $>10^{-4}$ mag/day represent a subset of the samples of QSO contaminants and their distribution in the colour–colour diagram is similar to that of the full samples (Fig. B.1).

By considering only sources with photometric errors <0.1 mag and quality flags =0 in each wave band, all YSOs are excluded (including the one above), only one star, a diffuse source and a PN remain in region B as well as two stars in region C while the number of background galaxies is also considerably reduced and confined within regions A and B, but for one source (Fig. B.1). The main criterion responsible for the removal of sources is the requirement on the quality flags. In fact, the magnitudes of most sources were extracted following a de-blending process corresponding to flag =16 (the confirmed QSO above has indeed this quality flag value in each VMC wave band). Since the Gruendl & Chu's sample is un-confirmed, the remaining galaxies are either QSO contaminants or QSO candidates themselves. These galaxies are not previously known, all but one have a well defined star-like appearance in the VMC images and about half of them have a slope of variation in the K_s band $>10^{-4}$ mag/day. The latter sample of high confidence QSO candidates, according to our criteria, has a 0% and 50% influence in region A and B, respectively, of QSO contaminants.

Appendix C: K_s band light-curves of known QSOs

Figure C.1 shows the K_s band light-curves of known QSOs in the presently available VMC data (observations acquired until end of September 2011) where single epoch data are included for completeness.

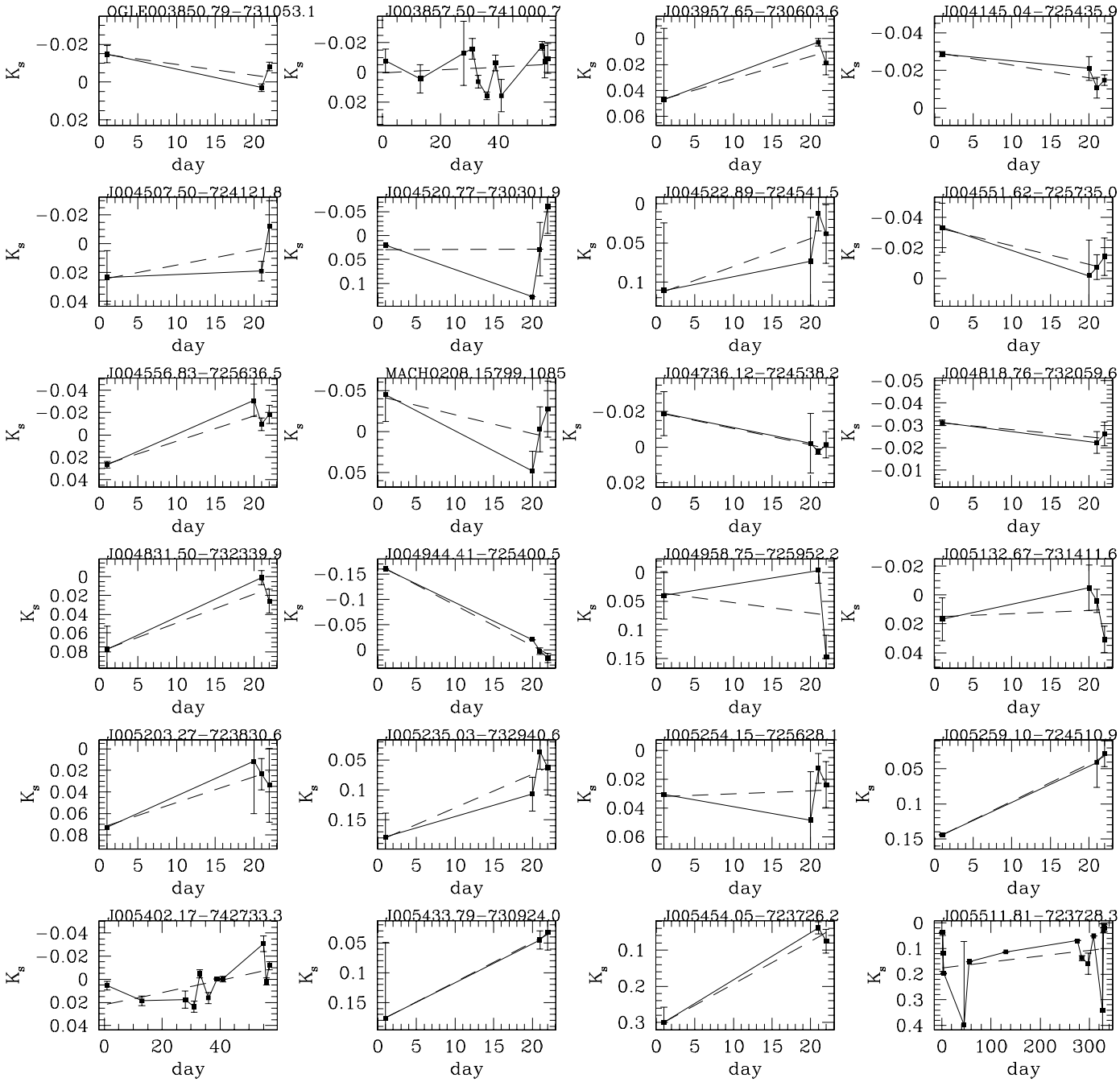

Fig. C.1. K_s band light-curves of known QSOs with respect to their mean magnitude. From *top to bottom and left to right* they follow the order in Table 2. Points represent the simple average of observations obtained within the same night/epoch and error bars correspond to the error of the mean. A continuous line connects the data points while a dashed line represents a linear fit through them. Day 0 corresponds to the first observation in the VMC data. Single epoch data are included for completeness.

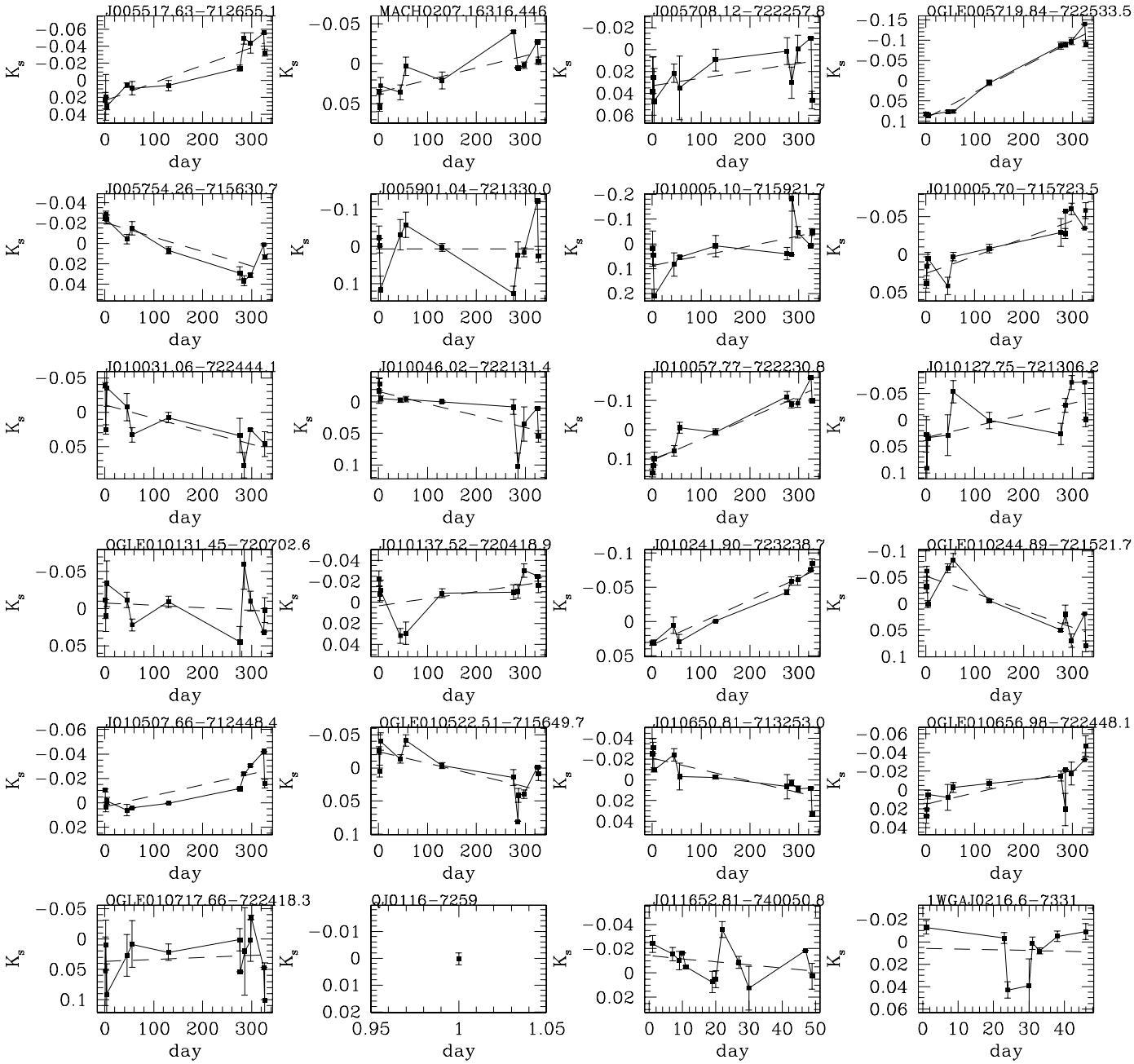

Fig. C.1. continued.

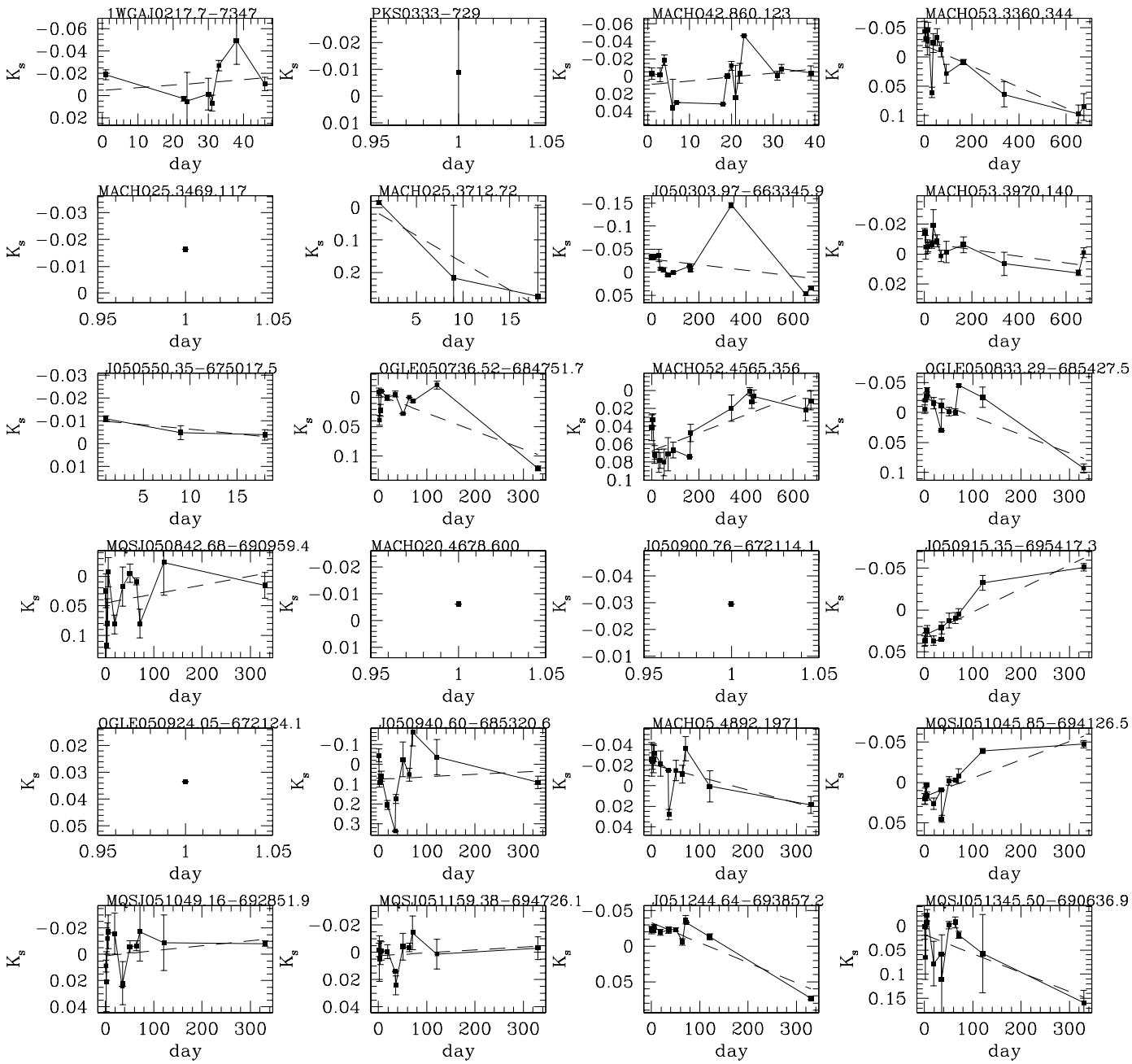

Fig. C.1. continued.

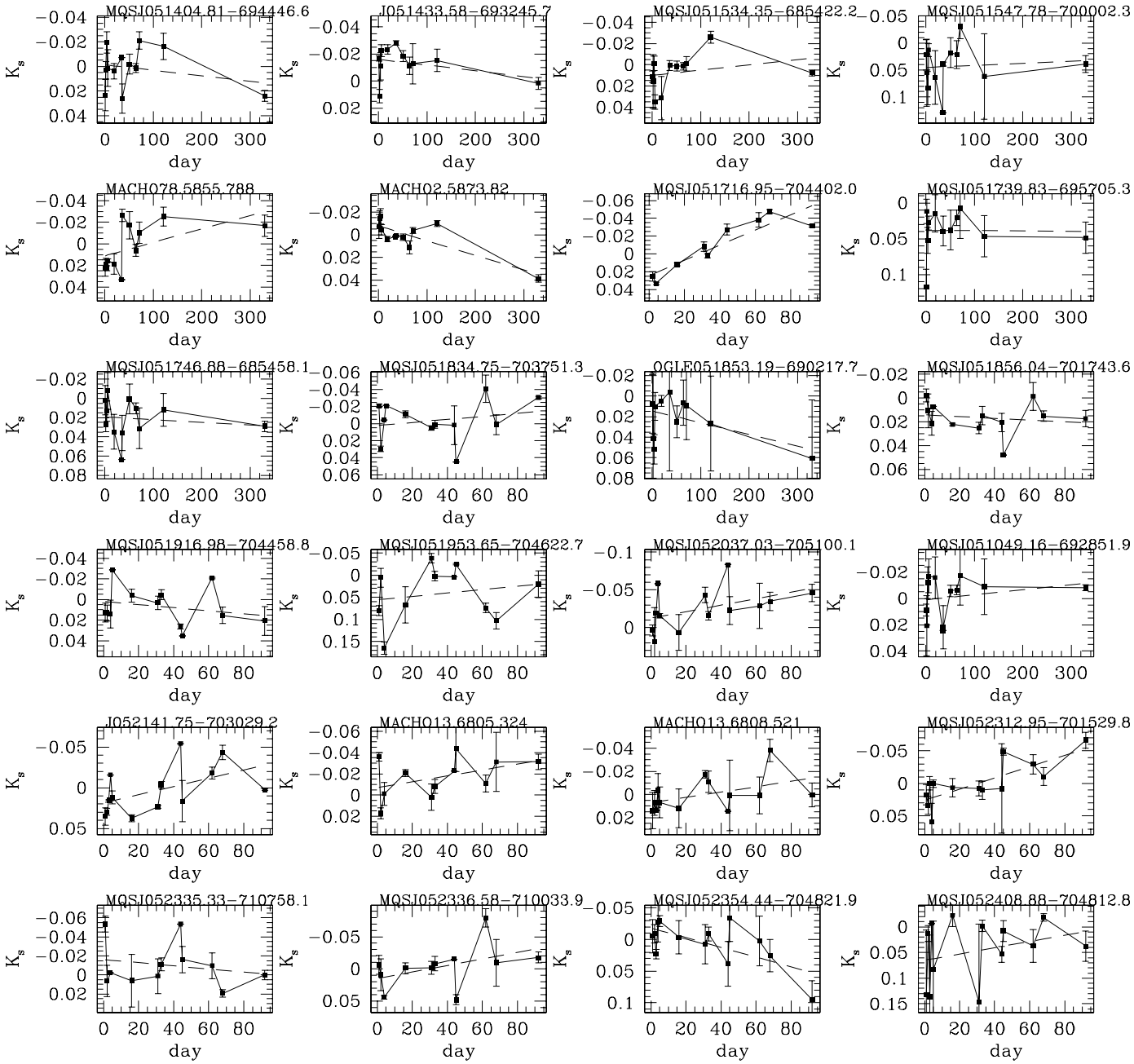

Fig. C.1. continued.

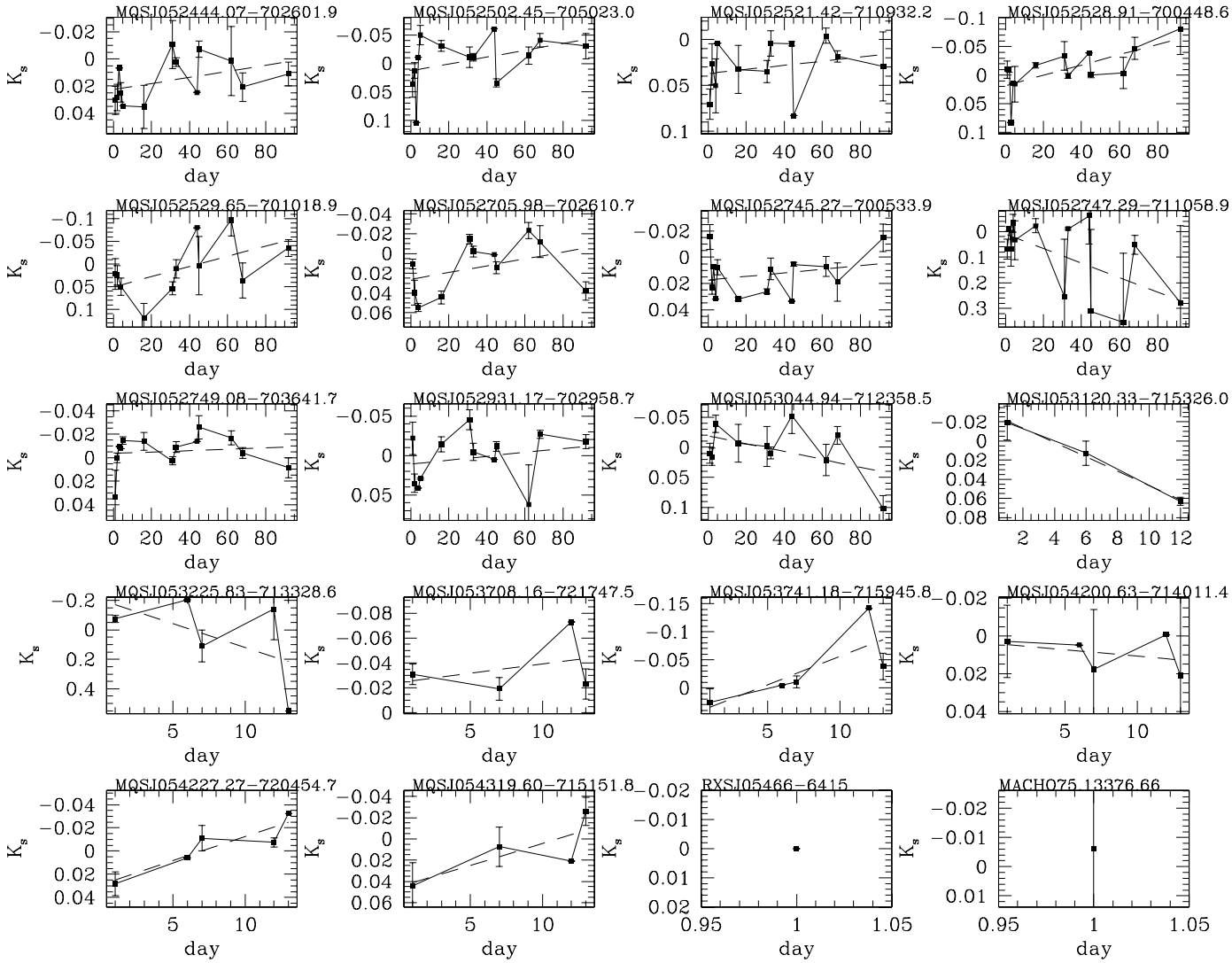

Fig. C.1. continued.